Available online at www.sciencedirect.com
ScienceDirect
Journal of Computational Physics 225 (2007) 1810–1826
JOURNAL OF COMPUTATIONAL PHYSICS
www.elsevier.com/locate/jcp

Tracking discontinuities in hyperbolic conservation laws with spectral accuracy

H. Touil, M.Y. Hussaini *, M. Sussman

School of Computational Science, Florida State University, Tallahassee, FL 32306, USA

Received 28 July 2006; received in revised form 19 February 2007; accepted 19 February 2007
Available online 27 February 2007

Abstract

It is well known that the spectral solutions of conservation laws have the attractive distinguishing property of infinite-order convergence (also called spectral accuracy) when they are smooth (e.g., [C. Canuto, M.Y. Hussaini, A. Quarteroni, T.A. Zang, Spectral Methods for Fluid Dynamics, Springer-Verlag, Heidelberg, 1988; J.P. Boyd, Chebyshev and Fourier Spectral Methods, second ed., Dover, New York, 2001; C. Canuto, M.Y. Hussaini, A. Quarteroni, T.A. Zang, Spectral Methods: Fundamentals in Single Domains, Springer-Verlag, Berlin Heidelberg, 2006]). If a discontinuity or a shock is present in the solution, this advantage is lost. There have been attempts to recover exponential convergence in such cases with rather limited success. The aim of this paper is to propose a discontinuous spectral element method coupled with a level set procedure, which tracks discontinuities in the solution of nonlinear hyperbolic conservation laws with spectral convergence in space. Spectral convergence is demonstrated in the case of the inviscid Burgers equation and the one-dimensional Euler equations.

Keywords: Discontinuous Galerkin; Spectral method; Front tracking; Level set; Ghost fluid method; Hyperbolic systems; Tracking method; Schemes; Fronts

1. Introduction

Numerical methods for treating shocked solutions of conservation laws can be classified into three categories – shock capturing, shock fitting and shock tracking. In a shock-capturing method, the shock is captured automatically by the discretization scheme and the explicit or implicit numerical dissipation (see [4] for an excellent review). In a shock-fitting method, a boundary-fitted co-ordinate system is used, and the shock is treated as a boundary, for which a separate evolution equation is derived and solved (e.g., [5,6]). In a shock-tracking method, the shock is "captured" and identified with a level set function, which is then tracked [7].

* Corresponding author. Tel.: +1 850 644 0601; fax: +1 850 645 1514.
E-mail address: michele@scs.fsu.edu (M.Y. Hussaini).

0021-9991/$ - see front matter
doi:10.1016/j.jcp.2007.02.016

A shock-capturing method based on spectral discretization exhibits global oscillations in the shocked solutions, known as Gibbs phenomenon [1–3], which usually causes numerical instability, particularly for nonlinear problems. Explicit numerical dissipation is required to obtain stable spectral solutions [8,9]. A stable spectral solution to the quasi-one-dimensional shocked flow was obtained with explicit numerical dissipation represented by a second-order viscous term discretized by central differences [8], and by a spectrally discretized hyperviscosity term [9]. However, spectral accuracy is obtained only away from the shock. Later, post-processing procedures, such as filters [10,11], were employed to smooth out the Gibbs oscillations. These artifacts degrade the spectral accuracy, at least in the vicinity of the shock. As Boyd [12] pointed out, it requires a spatially-adaptive filter whose order varies from small values in the neighborhood of the shock to large values in the smooth regions far away from the shock. To carry out such adaptive filtering, one needs a tool for identifying shocks that is spectrally accurate. There are two other types of post-processing procedures – spectral mollification, and Gegenbauer reconstruction (see [11,13] for critical reviews). The shock-fitting method [14,15] precludes Gibbs phenomenon and provides smooth solutions with spectral accuracy. However, topological difficulty arises in treating complex flow configurations with shocks that are not amenable to being contained in rectangular domains. As the level set formulation [16] has the flexibility to deal with complex topological changes arising in the evolution of curves and surfaces, the objective of the ongoing research has been to couple a level set procedure with the discontinuous spectral element method (DSEM) to deal with discontinuous solutions with spectral accuracy. As a first step towards this end, the effort reported in [17] developed a level set advection algorithm with spectral accuracy. Grooss and Hesthaven [18] propose a spectral Galerkin/level set method for free surface flows, but their ''smeared'' interface treatment at the discontinuity is only first-order accurate.

In this paper, we present a coupled discontinuous spectral element (DSEM)/level set method that yields uniformly spectral spatial convergence of the solution, including the shock speed and location. Specifically, the computational domain is divided into elements wherein the solution, if it is smooth, is represented by pth-order polynomials (and utilizes appropriate Gauss quadrature techniques). The elements containing a discontinuity (i.e., where the level set function ψ changes sign) are called Godunov elements. Each Godunov element is subdivided into 2^p subelements, and each subelement is treated with a first-order accurate method. So, the ''virtual'' order of accuracy in a Godunov element is proportional to $(1/2)^p$, which implies spectral accuracy. (Note that in principle, in order to obtain spectral accuracy, we can subdivide a Godunov element into the integer part of a^p subelements for any value of $a > 1$.)

The proposed method may be viewed in two different ways: it may be viewed as a form of (i) adaptive mesh refinement (AMR) [19–22] in which the mesh size h is refined or (ii) p refinement in which the order p of elements is increased. The distinction between the present method and previous methods based on either h refinement or p refinement is that the resulting order of accuracy (as distinguished from the ''formal'' order of accuracy) is ''optimal'' in that the order of accuracy of the proposed method is *uniformly* spectral. In other words, the accuracy of the solution in the regular elements as well as the ''virtual'' order of accuracy in the Godunov elements are both spectral. We remark that for conventional AMR implementations, one must implement complicated interpolation procedures when providing boundary conditions for the refined regions. In the present approach, we exploit the locally high-order accurate representation of the solution in the regular elements to provide boundary conditions for the Godunov elements. We use the piecewise-constant representation in Godunov elements for providing the boundary conditions for the regular elements. We also remark that the present method is distinct from the standard p refinement approaches as it does not retain the high order polynomial representation in the Godunov elements; instead it switches to piecewise constant interpolation in elements containing the zero level set. We emphasize that one must use the level set function to explicitly track the front, since shock capturing (or shock-detection) schemes do not ensure spectral accuracy for shock location.

2. Governing equations

The generic form for a conservation law is

$$\frac{\partial U}{\partial t}+\frac{\partial F(U)}{\partial x}+\frac{\partial G(U)}{\partial y}+\frac{\partial H(U)}{\partial z}=0, \tag{1}$$

where $U(x,y,z,t)$ is the conserved variable and F, G, and H are the fluxes in the x-, y- and z-directions, respectively. Eq. (1) may also be written in compact form,

$$\frac{\partial U}{\partial t} + \nabla \cdot \mathscr{F} = 0, \tag{2}$$

where $\mathscr{F} = (F, G, H)$.

Eq. (2) with a discontinuous solution is split into two smooth problems to exploit a level set procedure [23]:

$$\begin{aligned} &\frac{\partial U^{(1)}}{\partial t} + \nabla \cdot \mathscr{F}^{(1)} = 0, \quad U = U^{(1)} \quad \text{if } \psi < 0, \\ &\frac{\partial U^{(2)}}{\partial t} + \nabla \cdot \mathscr{F}^{(2)} = 0, \quad U = U^{(2)} \quad \text{if } \psi \geqslant 0, \end{aligned} \tag{3}$$

$$\frac{\partial \psi}{\partial t} + S(U^{(1)}, U^{(2)}, n)|\nabla \psi| = 0, \tag{4}$$

where ψ is the level set function, and $\psi = 0$ represents a singular surface, such as a shock wave whose normal n is given by

$$n = \frac{\nabla \psi}{|\nabla \psi|}$$

and whose speed S is obtained from solving the appropriate Riemann problem with the two states, $U^{(1)}$ and $U^{(2)}$. For a discontinuous solution of Eq. (2), one considers its weak form, which is obtained by multiplying it by an appropriate test function $v(x,y,z)$ and integrating the product over the whole domain Ω:

$$\frac{\partial}{\partial t}\int_\Omega Uv \,\mathrm{d}\Omega + \int_\Omega v \nabla \cdot \mathscr{F} \,\mathrm{d}\Omega = 0. \tag{5}$$

Integration by parts yields

$$\frac{\partial}{\partial t}\int_\Omega Uv \,\mathrm{d}\Omega + \int_{\partial\Omega} v\mathscr{F} \cdot n(\partial\Omega)\mathrm{d}\sigma - \int_\Omega \mathscr{F}(U)\nabla v \,\mathrm{d}\Omega = 0, \tag{6}$$

where $\partial\Omega$ is the boundary of Ω.

3. Solution technique

3.1. Spatial discretization: discontinuous spectral element method

The domain Ω of computation is divided into M hexahedral elements/subdomains Ω_m. On this grid Eq. (6) becomes

$$\frac{\partial}{\partial t}\sum_{m=1}^{M}\int_{\Omega_m} Uv \,\mathrm{d}\Omega + \sum_{m=1}^{M}\int_{\partial\Omega_m} v\mathscr{F} \cdot n(\partial\Omega_m)\mathrm{d}\sigma - \sum_{m=1}^{M}\int_{\Omega_m} \mathscr{F}(U) \cdot \nabla v \,\mathrm{d}\Omega = 0. \tag{7}$$

Each of the elements Ω_m is mapped $(f : (x,y,z) \to (\xi,\eta,\zeta))$ onto a master cube $[-1,1] \times [-1,1] \times [-1,1]$, wherein the conservation law variables U and the level set function ψ are represented in terms of the polynomial basis functions of order p:

$$U_m(x) = \sum_{i=0}^{p}\sum_{j=0}^{p}\sum_{k=0}^{p} U_m^{i,j,k} L_i(\xi) L_j(\eta) L_k(\zeta) \quad m \in [1, M], \tag{8}$$

where L_i are the Lagrange interpolants,

$$L_i(\xi) = \prod_{l=0, l\neq i}^{p} \frac{\xi - \xi_l^*}{\xi_i^* - \xi_l^*}. \tag{9}$$

The interpolation nodes ξ_l^* are the Chebyshev–Gauss–Lobatto (CGL) points defined by

$$\xi_l^* = -\cos\left(\frac{\pi l}{p}\right) \quad l \in [0,p]. \tag{10}$$

Clenshaw–Curtis quadrature [24,25] is used to discretize (6), wherein the quadrature nodes are determined by the Chebyshev–Gauss–Lobatto nodes and the quadrature formula is given by

$$\int_{\Omega_m} U \,\mathrm{d}\Omega \approx \sum_{i=0}^{p}\sum_{j=0}^{p}\sum_{k=0}^{p} U_m^{i,j,k} w_i w_j w_k,$$

where the weights, $w_i w_j w_k$, are determined by

$$w_i w_j w_k = \int_{\Omega_m} L_i(\xi) L_j(\eta) L_k(\zeta) \mathrm{d}\Omega.$$

As Trefethen [25] points out, "the Clenshaw–Curtis formula has essentially the same performance (as Gauss quadrature) for most integrands and can be implemented effortlessly by the FFT."

In the discontinuous spectral element method, rather than enforcing continuity at the interfaces of $\partial\Omega_m$ between the elements Ω_m, one instead solves a Riemann problem at these interfaces. We use local Lax–Friedrich (LLF) to compute the numerical fluxes,

$$\widetilde{F}^{\mathrm{Riem}}(U_{\mathrm{L}}, U_{\mathrm{R}}) n(\partial\Omega_m) = \frac{1}{2}\left[(\mathscr{F}(U_{\mathrm{L}}) + \mathscr{F}(U_{\mathrm{R}})) \cdot n(\partial\Omega_m) - \lambda_f^*(U_{\mathrm{R}} - U_{\mathrm{L}})\right]. \tag{11}$$

Here, U_{L} is the state derived from the interior of Ω_m, U_{R} the state derived from the exterior of Ω_m, and $n(\partial\Omega_m)$ is the outward facing normal to the element Ω_m, λ_{f}^* is the fastest wave speed arising in the conservation law, and * indicates that the quantity is computed using the average of U_{L} and U_{R}. For the Euler equation $\lambda_{\mathrm{f}}^* = (|u^*| + c^*)$, where u^* is the velocity and c^* is the speed of sound at the discontinuity.

It is but proper to mention here that the present method is the nodal version of the spectral discontinuous Galerkin (DG) method. However, the Runge–Kutta DG method [26] purports to have the same order of accuracy for both space and time. We call the present method a discontinuous spectral element method as it takes the same philosophy (but with the discontinuous Galerkin method as the fundamental approximation) as the commonly-acknowledged spectral element method originally developed by Patera [27]. It is expedient to use a nodal distribution (Chebyshev–Gauss–Lobatto as in the present instance or Legendre–Gauss–Lobatto distribution) that includes the boundary points so that the discrete locations of the conserved quantities and the level set function will be collocated. A nodal distribution that includes the boundary points ensures continuity of the level set function across element boundaries during the redistancing step [17].

3.2. Time discretization

The semi-discrete (after spatial discretization) form of Eq. (1) is

$$\frac{\partial U}{\partial t} = L(U,t).$$

The temporal derivative is discretized by the total variation diminishing (TVD) second-order Runge–Kutta method (also known as the Heun method):

$$\begin{aligned} U^* &= U^n + \Delta t L(U^n, t^n), \\ U^{n+1} &= \frac{1}{2}U^n + \frac{1}{2}U^* + \frac{1}{2}\Delta t L(U^*, t^n + \Delta t). \end{aligned} \tag{12}$$

It belongs to the general class of "strong stability preserving" time discretization schemes (SSP) [29]. The choice of second-order SSP was dictated by the relatively larger time step it permits compared to the third-order or fourth-order SSP Runge–Kutta time stepping method.

4. Spectral level set procedure

If a discontinuity lies exactly at the interface between two elements, the standard discontinuous spectral element method does not suffer from the Gibbs phenomenon, as the overall solution is allowed to be discontinuous across elements (where an appropriate Riemann problem is solved at the interface between elements). If a discontinuity lies inside an element, high-order polynomial interpolation, without the so-called "post-processing artifacts," gives rise to Gibbs phenomenon as mentioned earlier in Section 1. Instead of "post-processing" out the Gibbs oscillations after they occur, our strategy is to preclude them from occuring by a "ghost fluid" approach [23] customized to realize global spectral accuracy. It involves the division of a Godunov element containing a discontinuity (i.e., the zero level set) into piecewise-constant subelements so that the solution procedure in these elements corresponds to a first-order Godunov method. Then, the question arises as to the number of subelements and matching the solution accuracy in a Godunov element with that in the contiguous regular elements. These questions are addressed in Sections 5.1.1 and 5.1.2. It is to be noted that the present approach not only applies for level set tracking (as covered in this paper) but also for shock capturing. One could use a shock detector [30,31] to determine the elements that need to be treated as Godunov elements.

First of all, the level set function ψ (see Section 2) is initialized by setting its value to zero where the conservation law variable U (scalar or vector) presents a discontinuity (for convenience, we limit ourselves to track a single jump only). Let us define $\Gamma(t)$ as the location where $\psi = 0$, i.e., the location of the discontinuity. In the rest of the space domain ψ is set to a signed distance to the zero level set, positive upstream of the shock and negative downstream of the discontinuity. In other words,

$$\psi(x,t) = \begin{cases} + \min\limits_{x_I \in \Gamma(t)} |x - x_I| & \text{upstream,} \\ - \min\limits_{x_I \in \Gamma(t)} |x - x_I| & \text{downstream.} \end{cases}$$

ψ is evolved in time by the integration of Eq. (4) with the second-order Runge–Kutta scheme (Section 3.2). Since ψ is defined as a signed distance to the zero level set, Eq. (4) takes the form

$$\frac{\partial \psi}{\partial t} + S = 0, \tag{13}$$

where S is the normal speed of the discontinuity. Where the level set function ψ changes sign, S is taken as the speed given by the Riemann solver as a function of the downstream state, $U^{(1)}$, the upstream state, $U^{(2)}$, and the interface normal, $n = \frac{\nabla \psi}{|\nabla \psi|}$. Outside the region where ψ changes sign, S is either extrapolated or obtained from the solution of the Riemann problem between the local ghost state and the physical state. At each new Runge–Kutta time step ψ is reset as a signed distance function.

In Godunov elements containing the discontinuity, we replace the single conservation law (1), which is solved in terms of the single discontinuous variable U, with the coupled system (3) written in terms of the two continuous variables $U^{(1)}$ and $U^{(2)}$ (see Section 2). "Ghost" states must be defined in Godunov elements containing a discontinuity. In the region downstream of the shock, $\psi < 0$, a ghost upstream state for $U^{(2)}$ must be defined. In the region upstream of the shock, $\psi > 0$, a ghost downstream state for $U^{(1)}$ must be defined. In order to define the ghost states, the downstream state, $U^{(1)}$, is extrapolated using piecewise constant extrapolation to the upstream side, and the upstream state, $U^{(2)}$, is extrapolated to the downstream side. At each downstream node in the Godunov element, the Riemann problem is solved between the extrapolated upstream state, $U^{(2)\text{extrap}}$ and the downstream state, U_1. At each upstream node in the Godunov element, the Riemann problem is solved between the extrapolated downstream state, $U^{(1)\text{extrap}}$ and the upstream state, $U^{(2)}$. The Riemann problem determines all the intermediate states between the upstream state and the downstream state. For example, for a shock wave, all the characteristics move into the shock from the upstream side, which means the ghost upstream state, $U^{(2)\text{ghost}}$, becomes the extrapolated upstream state, $U^{(2)\text{extrap}}$. Only one characteristic moves into the shock from the downstream side, which means the ghost downstream state, $U^{(1)\text{ghost}}$, becomes the intermediate state that neighbors the upstream state, $U^{(2)}$. Fig. 1 illustrates the upstream and downstream states along with their corresponding ghost states.

Now, to clarify the details for the discretization in space $U^{(1)}$, $U^{(2)}$, and ψ they are primarily discretized by M spectral elements of order p in the whole spatial domain, as explained in Section 3. The exceptions are the

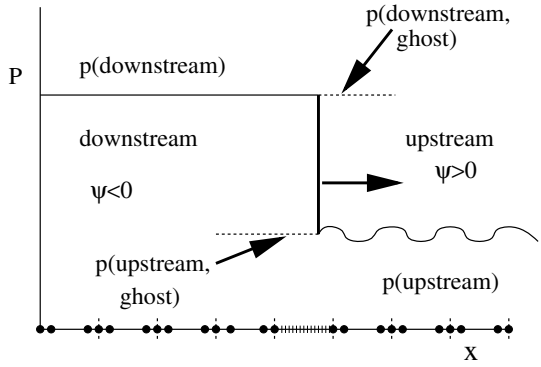

Fig. 1. Illustration of upstream and downstream states along with their corresponding ghost states.

Godunov elements I_{crit} containing the zero level set (i.e., the discontinuity), which are subdivided into $N \times N \times N$ uniform subelements. It is illustrated for the one-dimensional case in Fig. 2. In these Godunov elements, the solution is represented by piecewise constant basis functions instead of the polynomial basis functions $L_i(\xi)L_j(\eta)L_k(\zeta)$ of spectral elements. When a discontinuity enters a spectral element, the solution represented by polynomial basis functions is interpolated on the Godunov element, specifically at the centers of the subelements. The solution values in the element (previously Godunov) from which the discontinuity exited are interpolated back to the regular pth-order spectral element (using the Chebyshev–Gauss–Lobatto nodes with Lagrange basis); a piecewise linear interpolation is used between the center of the subelements. Fig. 3 illustrates this interpolation process in one dimension.

The interpolation procedures that we use to transfer data from a "Godunov" element to a spectral element and vice versa do not preserve discrete conservation. There will be an error on the order of $O(h^p)$ when transferring data from a spectral element to a Godunov element and an error on the order of $O(h/N)$ when transferring data back from a Godunov element to a spectral element, where p is the order of an element, h is size of an element and N the number of subelements (e.g., 2^p). Since the transfer operations are done at most, once per time step, the overall error from this operation will not deteriorate the overall spectral accuracy of the method. Also, the fact that conservation form is formally preserved for each separate region, upstream or downstream of the tracked shock, ensures that discontinuities in each region will be captured with the correct speed and amplitude. We remark that the standard ghost-fluid treatment of the "Godunov" elements does not preserve conservation either; but conservation is violated only at the tracked shock, whose shock speed is correctly determined from the associated Riemann

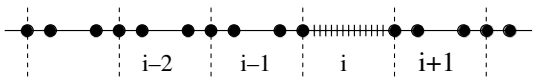

Fig. 2. Spectral elements of order $p = 3$ (four nodes) surrounding a Godunov element containing uniform subelements.

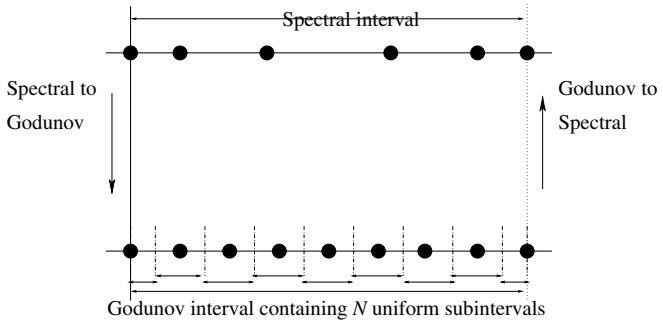

Fig. 3. Interpolation process when the discontinuity leaves a Godunov interval or enters a spectral interval.

problem, and it does not adversely affect the spectral accuracy of the present method. Conservation issues and viable fixes are discussed in a paper by Nguyen et al. [32], and they are applicable to the spectral ghost fluid approach.

Solving for U in the spectral elements (where the solution is represented in terms of polynomial basis functions) is straightforward. Briefly stated, we precompute the spectral weights for quadrature as well as the derivative matrix associated with the basis functions. The calculation of the derivative matrix requires special attention, particularly for high order polynomial representations (e.g., $p > 5$), due to round-off errors that accumulate during the calculation of the matrix coefficients. Here, we use a classical subtraction artifact to get the diagonal [33]. There are two ways to verify the consistency of the derivative matrix. The first one is to verify that the derivative of a constant function f in the element interval is equal to zero:

$$\frac{\partial f(\xi_i, \eta_j, \zeta_k)}{\partial \xi} = \sum_{l=0}^{p} \sum_{m=0}^{p} \sum_{n=0}^{p} f_{i,j,k} L_l'(\xi_i) L_m(\eta_j) L_n(\zeta_k) = 0. \tag{14}$$

This leads to the relation

$$\sum_{j=0}^{p} L_j'(\xi_i) = 0. \tag{15}$$

The subtraction artifact consists in computing all the extradiagonal terms $L_j'(\xi_i)$ $(i \neq j)$ and to get the diagonal term by subtraction:

$$L_i'(\xi_i) = -\sum_{j=0, j\neq i}^{p} L_j'(x_i). \tag{16}$$

In the context of integration by quadrature, we introduce a new consistency condition. The derivative matrix has to verify

$$\int_{\xi_0}^{\xi_p} L_i'(\xi) \mathrm{d}\xi = \sum_{j=0}^{p} L_i'(\xi_j) w_j = [L_i(\xi_p) - L_i(\xi_0)] = [\delta_{pj} - \delta_{0j}], \tag{17}$$

where the w_j are the known (precomputed) weights of the quadrature.

We now summarize the spectral level set procedure.

Tracker algorithm

1: Give $U^{(1)}(x,0)$, $U^{(2)}(x,0)$ and $\psi(x,0)$
2: time $= 0$
3: **repeat**
4: time $=$ time $+ \Delta t$
5: **if** shock exits or enters an element {see Fig. 2} **then**
6: interpolate the spectral element on the "Godunov" subelements
7: interpolate back the element wherefrom shock exited ("Godunov") to spectral element (linear interpolation between the nodes).
8: **end if**
9: calculate the advection speed U
10: solve for the smooth problems Eqs. (4) and (3)
11: reinitialize ψ to be a distance function. ψ is linearly interpolated to find the zero, and then set to $x - X0$, where $X0$ is the position of the discontinuity.
12: extrapolation of the values of $U^{(1)}$ and $U^{(2)}$ in their respective ghost regions
13: **until** (stopping criterion)

Although the present work is confined to one dimension, the extension to multi-dimensions is technically straightforward, as the ghost fluid treatment that we apply to the "Godunov" subelements has already been extended to multidimensional problems [23]. Perhaps, some experimentation is required in multiple dimensions in order to verify uniform spectral accuracy as the elements intersect at more than one node.

5. Numerical results

The discontinuous spectral element method is applied to the inviscid Burgers equation and the one-dimensional Euler equations. The spectral convergence of the method is examined in terms of the following error norms.

Let us assume one has a discrete representation of the exact solution with N evenly spaced points (U_i^{exact}, $i = 1 \ldots N$). To compare the DSEM solution with the exact solution, the DSEM solution (on M spectral elements of order p and Godunov element) is appropriately interpolated on any of the N evenly spaced points (assuming $N \gg Mp$): U_i^{hp}, $i = 1 \ldots N$. Then the classical formulas for the l_1, l_2 and l_∞ error norms yield:

$$l_1 = \frac{1}{N}\sum_{i=1}^{N} |U_i^{\text{exact}} - U_i^{hp}|,$$

$$l_2 = \sqrt{\frac{1}{N}\sum_{i=1}^{N} (U_i^{\text{exact}} - U_i^{hp})^2},$$

$$l_\infty = \max_{i=1\ldots N} |U_i^{\text{exact}} - U_i^{hp}|.$$

5.1. Inviscid burgers equation

We consider the periodic solution of the inviscid Burgers equation on the interval $[-2.5, 7.5]$

$$\frac{\partial u}{\partial t} + \frac{\partial}{\partial x}\left(\frac{u^2}{2}\right) = 0. \tag{18}$$

The initial condition is (see Fig. 4)

$$u(x,0) = \begin{cases} 1 & \text{if } x \leqslant -1, \\ 1 + \frac{1}{8}(1 + \cos(\pi x)) & \text{if } x > -1 \text{ and } x \leqslant 0, \\ 1 - \frac{1}{8}(1 + \cos(\pi x)) & \text{if } x > 0 \text{ and } x \leqslant 1, \\ 1 & \text{if } x > 1. \end{cases} \tag{19}$$

Eq. (18) with a discontinuous solution is split into two smooth problems:

$$\begin{aligned} &\frac{\partial u^{(1)}}{\partial t} + \frac{\partial}{\partial x}\left(\frac{[u^{(1)}]^2}{2}\right) = 0, \quad u = u^{(1)} \quad \text{if } \psi < 0, \\ &\frac{\partial u^{(2)}}{\partial t} + \frac{\partial}{\partial x}\left(\frac{[u^{(2)}]^2}{2}\right) = 0, \quad u = u^{(2)} \quad \text{if } \psi \geqslant 0, \end{aligned} \tag{20}$$

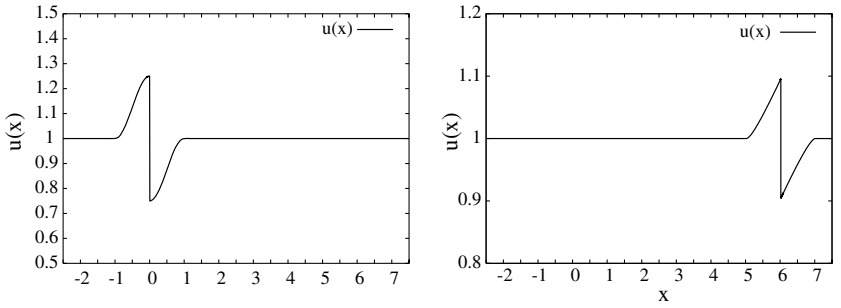

Fig. 4. Initial and final solution of Eq. (18) based on 100 elements with 11th-order polynomial representation in each element.

$$\frac{\partial \psi}{\partial t} + S(u^{(1)}, u^{(2)}) \left| \frac{\partial \psi}{\partial x} \right| = 0, \tag{21}$$

with initial conditions

$$u^{(1)}(x,0) = \begin{cases} 1 & \text{if } x \leqslant -1, \\ 1 + \frac{1}{8}(1 + \cos(\pi x)) & \text{if } x > -1 \text{ and } x \leqslant 0, \\ 5/4 & \text{if } x > 0, \end{cases} \tag{22}$$

$$u^{(2)}(x,0) = \begin{cases} 3/4 & \text{if } x \leqslant 0, \\ 1 - \frac{1}{8}(1 + \cos(\pi x)) & \text{if } x > 0 \text{ and } x \leqslant 1, \\ 1 & \text{if } x > 1, \end{cases} \tag{23}$$

$$\Psi(x,0) = x. \tag{24}$$

Here ψ is the level set function, and $\psi = 0$ represents the discontinuity.

The speed of the discontinuity, $S(u^{(1)}, u^{(2)})$, is

$$S = \frac{[f(u)]}{[u]} = \frac{f(u^{(2)}) - f(u^{(1)})}{u^{(2)} - u^{(1)}}, \tag{25}$$

where $f(u) = \frac{u^2}{2}$.

In this case, it is easy to define the "ghost" states for $u^{(1)}$ and $u^{(2)}$. Since the characteristic from the downstream side, $\psi < 0$, moves into the discontinuity, and the characteristic from the upstream side, $\psi > 0$, also moves into the discontinuity, we have $u^{(1)\text{ghost}} = u^{(1)\text{extrap}}$ and $u^{(2)\text{ghost}} = u^{(2)\text{extrap}}$. Stated otherwise, suppose $\psi = x - X0$ where $X0$ is the position of the discontinuity, then

$$u^{(1)} = \begin{cases} u^{(1)}(x) & x < X0, \\ u^{(1)}(X0^-) & x > X0 \text{ (ghost region 1)}, \end{cases} \tag{26}$$

$$u^{(2)} = \begin{cases} u^{(2)}(x) & x > X0, \\ u^{(2)}(X0^+) & x < X0 \text{ (ghost region 2)}. \end{cases} \tag{27}$$

The solution technique discussed in Sections 3.1 and 3.2 is applied to this one-dimensional scalar case. The computational domain $[-2.5, 7.5]$ is divided into M intervals on which Eqs. (20) and (21) for $u^{(1)}$, $u^{(2)}$ and ψ are discretized using the spatial discretization (7) (written in a generic form):

$$\frac{\partial u_m}{\partial t} = R_m(u_m, f_m^{\text{Riem}-}, f_m^{\text{Riem}+}, t), \tag{28}$$

where u_m is the solution in the mth interval and f^{Riem} is the Riemann flux on the interfaces with

$$\begin{aligned} f_m^{\text{Riem}-} &= f^{\text{Riem}}(u_{m-1}(1), u_m(-1)), \\ f_m^{\text{Riem}+} &= f^{\text{Riem}}(u_m(1), u_{m+1}(-1)). \end{aligned} \tag{29}$$

We use the local Lax–Friedrich (LLF) to compute the numerical fluxes,

$$f^{\text{Riem}}(U_{\text{L}}, U_{\text{R}}) = \frac{1}{2}\left[f(U_{\text{L}}) + f(U_{\text{R}}) - \lambda_{\text{f}}^*(U_{\text{R}} - U_{\text{L}})\right], \tag{30}$$

where U_{L} and U_{R} are the values at the left and at the right of the discontinuity.

we apply the TVD Runge–Kutta method (12) for the temporal derivative.

For clarity, we reiterate the details in the one-dimensional scalar case. The solution is represented by polynomials of order p in all the intervals except the ones in which the solution is discontinuous. The former are called spectral intervals and the latter are called Godunov intervals. The Godunov intervals (which by definition contain the zero level set) are subdivided into N uniform subintervals as illustrated in Fig. 2.

In the Godunov intervals, the upstream solution and the downstream solution are represented separately by piecewise constant basis functions instead of the polynomial basis functions L_i of spectral inter-

vals. When a discontinuity enters a spectral interval, the upstream and the downstream solutions, currently represented by polynomial basis functions, are interpolated on the centers of the subintervals. The solution values in the interval (previously Godunov) from which the discontinuity exits are interpolated back to the regular pth-order spectral element (using the Chebyshev–Gauss–Labatto nodes with Lagrange basis); a piecewise linear interpolation is used between the centers of the subintervals. The following equation describes the interpolation procedure (in one dimension) to a newly formed "Godunov" element point, ξ_G,

$$u(\xi_G) = \sum_{i=0}^{p} u_m^i L_i(\xi_G).$$

We use simple linear interpolation to initialize spectral nodes that were previously contained in a "Godunov" element. This interpolation process is illustrated in Fig. 3: on top is a fifth-order spectral element (six nodes). The spectral solution values in this interval are interpolated on the N evenly spaced nodes of the bottom Godunov interval. The boundaries of the new subintervals are exactly between these nodes (boundary locations are where the numerical fluxes are computed).

The CFL condition for the TVD Runge–Kutta method is

$$\Delta_t \leqslant C_{\mathrm{cfl}} \frac{\Delta_x}{U_{\mathrm{cfl}}},$$

where Δ_t is the time-step for the computation, Δ_x is the smallest distance between two computational nodes and U_{cfl} is the fastest wave speed arising in the computation. The CFL coefficient C_{cfl} is theoretically equal to one in Eq. (12). Keeping in mind that the ratio $\Delta_x/U_{\mathrm{cfl}}$ may have round-off error, we set the value of C_{cfl} at 0.99. The additional time-step constraint imposed by a Godunov element, due to its 2^p subelements, is given by the ratio of the shortest distances between two Godunov subelements and two spectral nodes, respectively:

$$\left(1 - \cos\frac{\pi}{p}\right) 2^{p-1}.$$

For example, when $p = 8$, the ratio is 9.7. To overcome this constraint, one could try sub-cycling techniques in the Godunov element. However, it should be noted that to obtain comparable accuracy using first-order subelements everywhere, one has to use at least $(M)(2^p)$ subelements, which will stringently constrain the time-step any way.

The following computations are based on 100 spatial intervals and a fixed time step so as to satisfy the CFL condition for the highest polynomial order of spectral representation. It remains to specify the number of subdivisions of the Godunov interval, which is discussed in the following section.

5.1.1. Choice for the number of Godunov subintervals

The smallest distance between two Chebyshev–Gauss–Lobatto points is proportional to p^{-2}. One could reason that the Godunov subinterval size should be proportional to p^{-2}, if one chooses the number of subintervals in a Godunov interval to be proportional to p^2 for the sake of consistency with the space between the nodes on the edge and close to the edge of the spectral intervals.

Eq. (18) defined in the previous subsection is integrated until time $t = 6.02$ for polynomial orders $p \in [2, 15]$. The error for the shock location and the global error in the l_1, l_2 and l_∞ norms are plotted in Fig. 5. The global error decays exponentially in all norms. However, only second-order convergence is observed for the shock location. One would not expect better than algebraic convergence (mth-order accuracy) for the front position if the number of Godunov subintervals N is proportional to p^m for arbitrary m. For instance, p^4 subelements yield fourth-order convergence (Fig. 6).

Since the zero level set or the shock is always confined to a Godunov element, the accuracy of its location will always be of $O(h/N)$, where h is the size of the element and N is the number of its subelements. In order to realize spectral accuracy for the shock location, N must be on the order of a^p. Otherwise, the position of the shock converges algebraically. One may speculate that the residence time of the shock in any computational

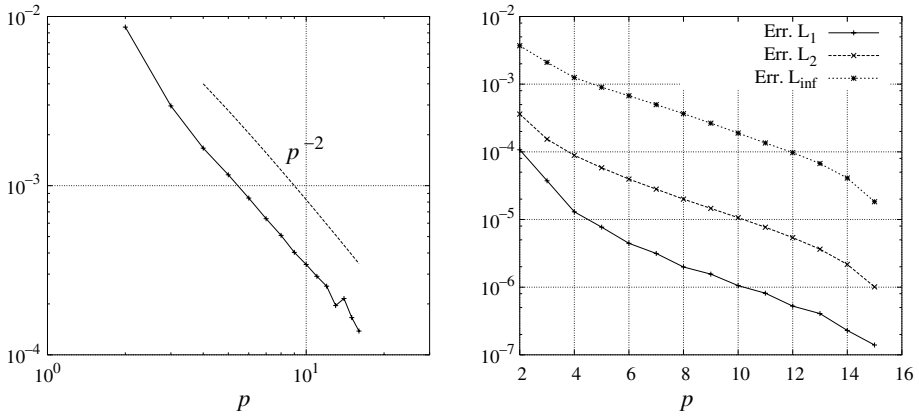

Fig. 5. Convergence of the position of the shock (left), and l_1, l_2 and l_∞ norms of the pointwise error (right): p^2 subintervals in the Godunov interval that contains the shock.

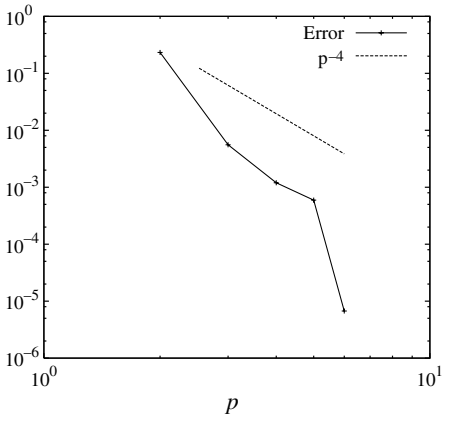

Fig. 6. Convergence of the position of the shock error: p^4 subintervals in the Godunov interval that contains the shock.

element is too small to degrade the solution from spectrally accurate to the $O(h/N)$ error present in a Godunov element.

5.1.2. Optimal choice for the number of Godunov subintervals for spectral accuracy

In order to obtain a spectral convergence for shock location, one has to get the associated error to behave as r^p, where r is the rate of convergence of the spectral method and p the order. Here we propose to split the Godunov interval containing the shock into 2^p subintervals. Polynomials of order $p \in [2, 8]$ are considered. The error for the location of the shock and the global error in the l_1, l_2 and l_∞ norms are plotted as functions of p in Fig. 7. The error decays exponentially in all norms (Fig. 7, right). The expected spectral convergence for the position of the shock is now achieved. The time step due to the CFL constraint decreases faster than the p^{-2} of the original spectral method. Despite that, as the spectral convergence is much faster than in the previous proposition (p^2 subintervals) and thanks to the $h - p$ flexibility of the discontinuous spectral element approach, many application will find this method valuable when a highly accurate solution is desired for problems with strong discontinuities.

5.2. Euler equations: Shu–Osher problem

The Shu and Osher problem [34] consists of the one-dimensional unsteady compressible Euler equations on the interval $x \in [-5, 5]$:

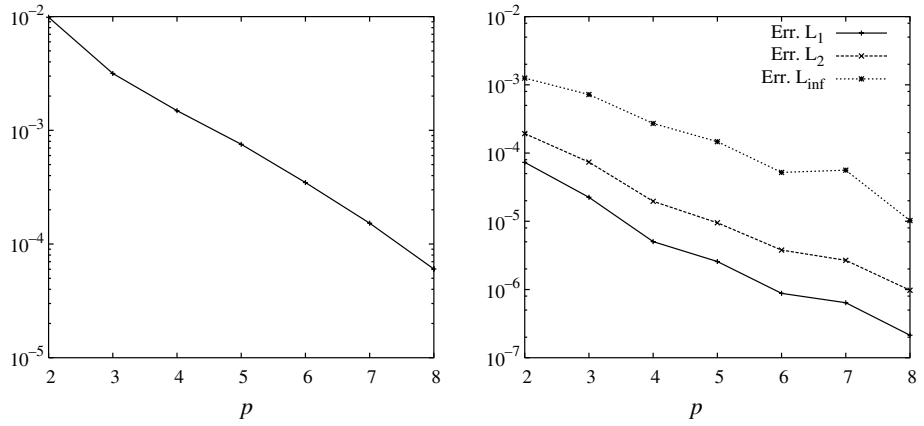

Fig. 7. Convergence of shock position, and l_1, l_2 and l_∞ norms of the pointwise error; 2^p subintervals in the Godunov interval.

$$\frac{\partial U}{\partial t}+\frac{\partial F(U)}{\partial x}=0, \tag{31}$$

with the equation of state,

$$pr=(\gamma-1)\left(E-\frac{1}{2}\rho u^2\right). \tag{32}$$

and the initial conditions,

$$\begin{aligned} &\rho_1(x,0)=3.857143, \qquad \rho_2(x,0)=1.+A\sin(\omega x)\\ &u_1(x,0)=2.629369, \qquad u_2(x,0)=0.\\ &pr_1(x,0)=10.333333, \quad pr_2(x,0)=1. \end{aligned}$$

Here, $U=\{\rho,\rho u,E\}^{\mathrm{T}}$ and $F(U)=\{\rho u,\rho u^2,u(E+pr)\}^{\mathrm{T}}$ where ρ, u, E and pr represent the density, velocity, total energy and pressure, respectively; A is the amplitude of the perturbation and $\omega/2\pi$ is its frequency. The subscripts 1 and 2 correspond, respectively, to the initial left (high pressure side) and right states of a shock initially located at $x=-4$.

For a system of conservation laws, as in the present instance of the Euler equations, the extrapolated states in the ghost regions are slightly less straightforward to deduce than for Burgers equation. Fig. 8 shows the wave pattern arising between the two states $U_{\mathrm{L}}=U_1(X0^-)$ and $U_{\mathrm{R}}=U_2(X0^+)$. These left and right values are used to solve the "exact" Riemann problem, providing the transport speed of the level set equation and the intermediate values U^*_{L} and U^*_{R}. They are separated by a left shock/rarefaction wave, a contact dis-

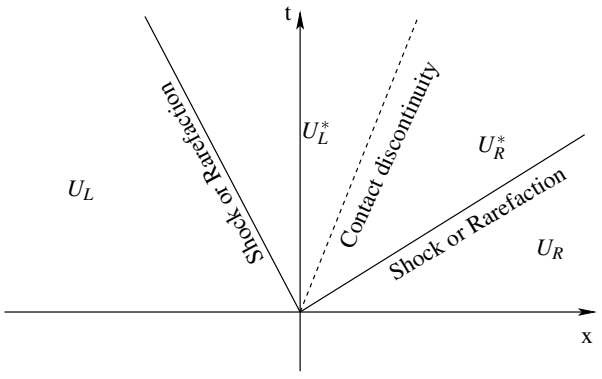

Fig. 8. Riemann wave pattern for Euler equations.

continuity wave and a right shock/rarefaction wave. If one is tracking a rightward moving shock, the ghost region of U_1 will take the value U_R^* since only one characteristic on the downstream side of the shock moves into the shock. The ghost region of U_2 will take the value $U_2(X0^+)$ (i.e., U_2^{extrap}) since all characteristics on the upstream side of the shock move into the shock. In other words we have

$$U_1 = \begin{cases} U_1(x) & x < X0, \\ U_R^* & x > X0 \text{ (ghost region 1)}, \end{cases}$$
$$U_2 = \begin{cases} U_2(x) & x > X0, \\ U_2(X0^+) & x < X0 \text{ (ghost region 2)}. \end{cases}$$

In this case the transport speed of the zero level set is the speed of the right going wave. More details concerning the choice of the left and right state are explained in [23].

Case I: $A = 0.2$ and $\omega = 5$.
The present spectral level set method is applied to the initial strong shock with the choice of 2^p subdivisions of the Godunov element where p is the order of the spectral element.

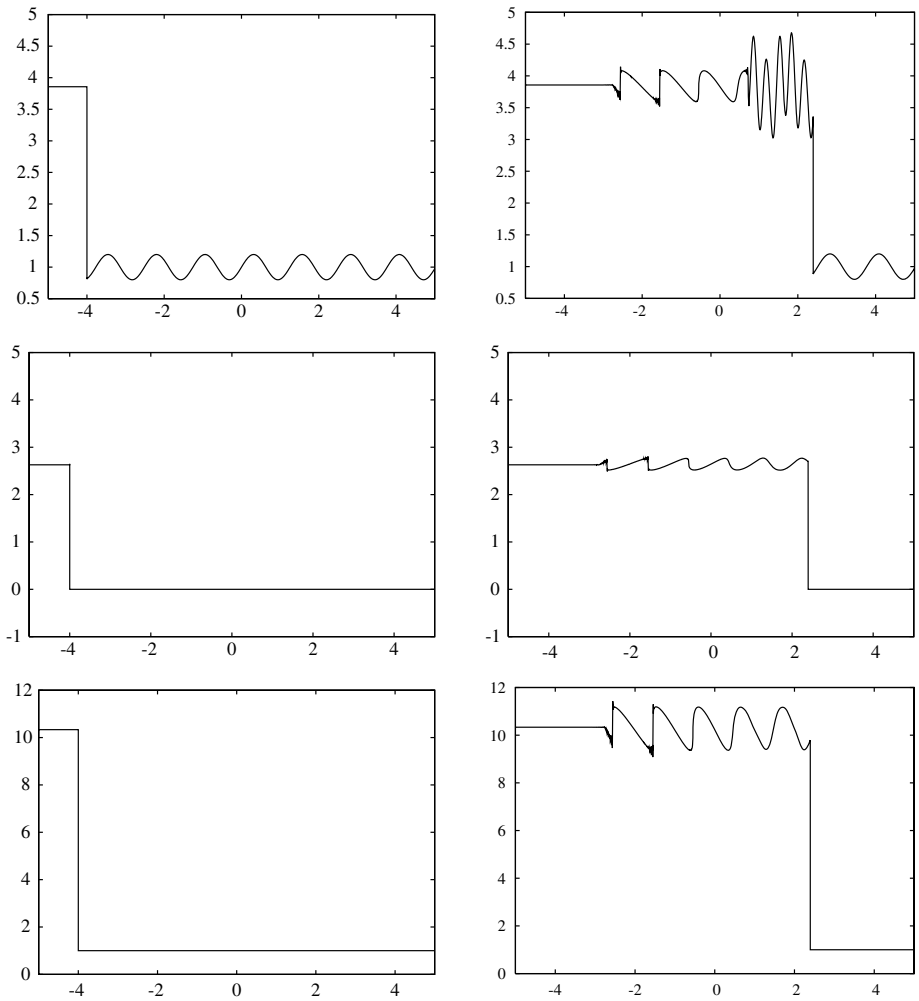

Fig. 9. Initial state (left) and final solution (right); top to bottom: ρ, u and 9i; 41 elements with 11th-order polynomial representation in each.

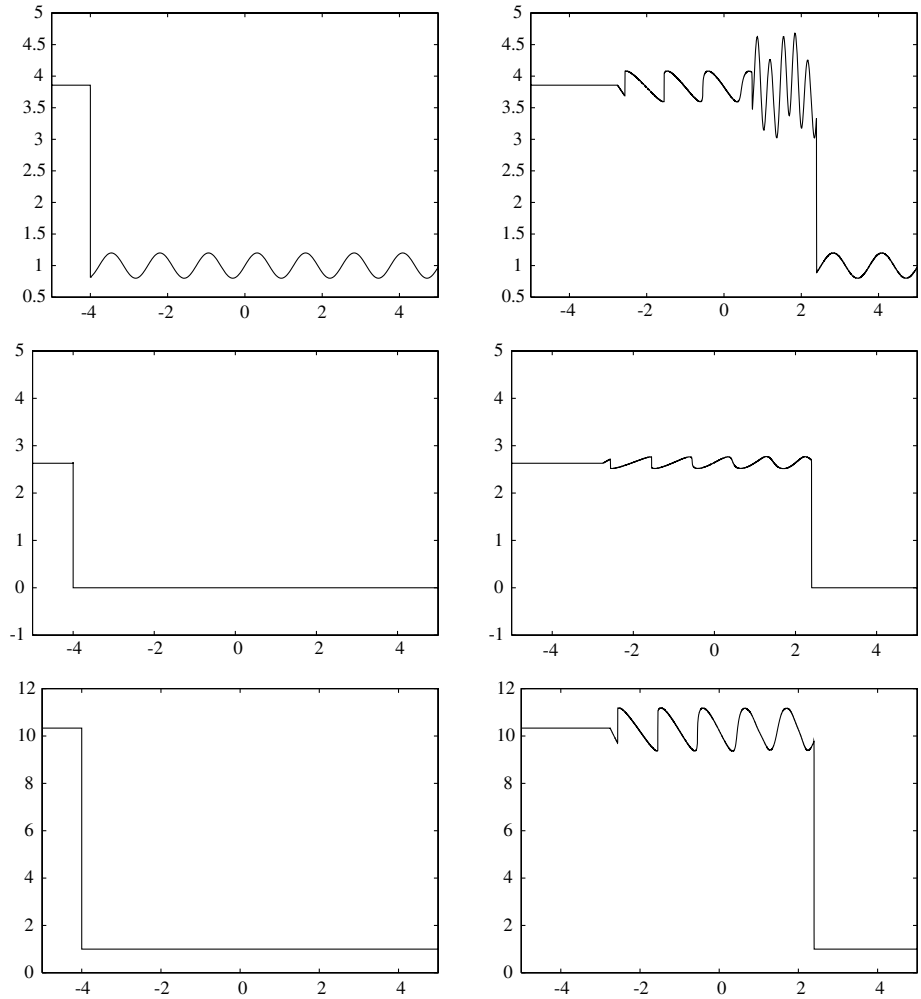

Fig. 10. Initial state (left) and final "exact" solution (right) corresponding to the approximate solution shown in Fig. 9; top to bottom: ρ, u and p; fifth-order WENO on 12,000 elements.

Fig. 9 shows the results at time $t = 1.8$ s. One can see the evolution of flow structures behind the shock as it interacts with the density disturbance. The solution is smooth and accurate in the vicinity of the primary shock that we actually track. As the waves propagate upstream of the shock, they steepen to form shocklets (weak discontinuities in ρ, u and p). These shocklets are not tracked and one can observe high frequency oscillations (Gibbs phenomenon) appearing in their immediate neighborhood. For eye-ball comparison, the corresponding solution obtained by WENO on 12,000 cells is displayed in Fig. 10. Fortunately, the method does not propagate these oscillations beyond the local element and one can expect a spectral convergence for the location of the strong shock. This is borne out in Fig. 11, where the error (with respect to the "numerically exact" solution of Greenough and Rider [35]) for the shock location is represented as a function of the polynomial order of the spectral elements. The method is actually found to be superconvergent.

One way to eliminate the Gibb's phenomenon associated with the "shocklets" observed in Fig. 9 is to implement a shock detector [30,31] and once detected, they can be contained in Godunov elements.

Case II: $A = 0.2$ and $\omega = 5\pi$.

These initial conditions evolve into a wave pattern and shocklets. The left graph in Fig. 12 displays a comparison of the result for density in the wave-pattern region $x \in [1, 2]$, (obtained by the spectral

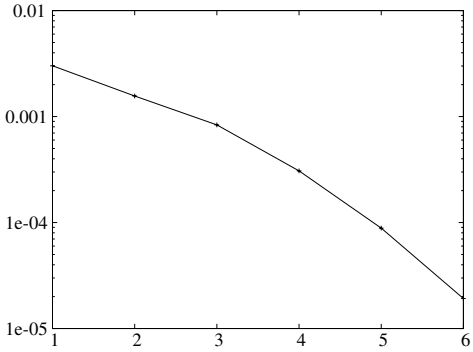

Fig. 11. Shu–Osher problem: shock location error.

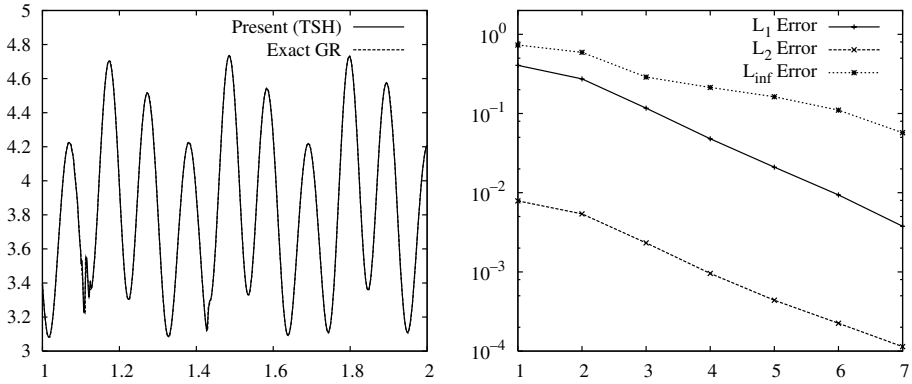

Fig. 12. Shu–Osher problem revisited; left: density as a function of x, spectral level set method (eighth-order) compared to Greenough and Rider "numerically exact" solution in the interval $x \in [1,2]$; right: convergence of l_1, l_2 and l_∞ errors in density as functions of the order p, $x \in [1,2]$; 200 elements; 2^p subelements in the interval with the shock.

level set method of order $p = 8$ with 200 elements) and the "numerically exact" solution of Greenough and Rider [35] based on 25,600 cells. (It must be mentioned that although the initial upstream density specified in [35] is $\rho_2(x,0) = 1.0 - A\sin(\omega x)$, the "numerically exact" data provided to us is for the case $\rho_2(x,0) = 1.0 + A\sin(\omega x)$, which is the expression we use).

The right graph in Fig. 12 shows the density error convergence in l_1, l_2 and l_∞ norms in the interval ($x \in [1,2]$) as functions of the polynomial order p. Two hundred elements are used to discretize the whole domain ($x \in [-5,5]$) and 2^p subelements in the shock region. We get clear spectral convergence for the l_1, l_2 and l_∞ norms. Although the convergence of the l_∞ error is spectral, it is relatively slower than the others.The present method requires $(M-1)*(p+1)+2^p = 199*9+2^8 = 2047$ nodes to be as accurate as (even possibly more accurate than) one of the best present shock-capturing methods, which requires 25,600 nodes. For a given accuracy, one may reasonably expect a gain of one order of magnitude in computational time, and even possibly three orders of magnitude in a suitable scenario.

6. Conclusion

A coupled discontinuous spectral element/level set method has been developed to solve the conservation laws with discontinuous solutions. Its spectral accuracy has been demonstrated in the case of shocked solutions of the Burgers equation and the system of one-dimensional compressible Euler equations. This method does not restrict its extension to include multidimensions and multiphase flows, and this will be the subject of

future efforts. Future work will also focus on the performance of the method as a function of the solution representation in the so-called Godunov elements that contain the zero level set. Presently, uniform spectral accuracy is obtained by subdividing a Godunov element into 2^p subelements, (where p is order of the contiguous spectral elements), where a monotonic first-order scheme is used. It will be of interest to explore the impact on accuracy and performance of the coupled method if a total variation diminishing scheme or an essentially nonoscillatory scheme were to replace the Godunov scheme. Of particular importance is the question of whether such a high-order scheme will require relatively less subelements for spectral accuracy.

Acknowledgments

The authors thank J.A. Greenough and W.J. Rider for providing the high resolution data used in Fig. 12.

References

[1] C. Canuto, M.Y. Hussaini, A. Quarteroni, T.A. Zang, Spectral Methods for Fluid Dynamics, Springer-Verlag, Heidelberg, 1988.
[2] J.P. Boyd, Chebyshev and Fourier Spectral Methods, second ed., Dover, New York, 2001.
[3] C. Canuto, M.Y. Hussaini, A. Quarteroni, T.A. Zang, Spectral Methods: Fundamentals in Single Domains, Springer-Verlag, Berlin Heidelberg, 2006.
[4] P.R. Woodward, P. Colella, The numerical simulation of two-dimensional fluid flow with strong shocks, Journal of Computational Physics 54 (1984) 115–173.
[5] G. Moretti, Computation of flows with shocks, Annual Review of Fluid Mechanics 19 (1987) 313–338.
[6] F. Marconi, M.D. Salas, Computation of three dimensional flows about aircraft configurations, Computers and Fluids 1 (1981) 185–195, 253.
[7] J. Glimm, H.L. Li, Y. Liu, N. Zhao, Conservative front tracking and level set algorithms, Proceedings of National Academy Sciences 98 (2001) 14198–14201.
[8] T.A. Zang, M.Y. Hussaini, Mixed spectral/finite difference approximations for slightly viscous flows, Lecture Notes in Physics 141 (1981) 461–466.
[9] A. Gelb, E. Tadmor, Enhanced spectral viscosity approximations for conservation laws, Applied Numerical Mathematics 33 (2000) 3–21.
[10] M.Y. Hussaini, D.A. Kopriva, M.D. Salas, T.A. Zang, Spectral methods for the Euler equations I: Fourier method and shock capturing, AIAA Journal 23 (1) (1985) 64–70.
[11] S.A. Sarra, Digital total variation filtering as post-processing for Chebyshev pseudospectral methods for conservation laws, Numerical Algorithms 41 (2006) 17–33.
[12] J.P. Boyd, The Erfc-Log filter and the asymptotics of the Euler and Vandeven sequence accelerations, in: Proceedings of the Third International Conference Spectral High Order Meth., published by Houston Journal of Mathematics, 1996, pp. 267–276.
[13] D. Gottlieb, C.W. Shu, On the Gibbs phenomenon and its resolution, Siam Review 39 (4) (1997) 644–668.
[14] M.Y. Hussaini, D.A. Kopriva, M.D. Salas, T.A. Zang, Spectral methods for the Euler equations II: Chebyshev method and shock fitting, AIAA Journal 23 (2) (1985) 234–240.
[15] D.A. Kopriva, T.A. Zang, M.Y. Hussaini, Spectral methods for the Euler equations: the blunt body problem revisited, AIAA Journal 29 (9) (1991) 1458–1462.
[16] S. Osher, J.A. Sethian, Fronts propagating with curvature-dependent speed: algorithms based on Hamilton–Jacobi formulations, Journal of Computational Physics 79 (1) (1988) 12–49.
[17] M. Sussman, M.Y. Hussaini, A discontinuous spectral element method for the level set equation, Journal of Scientific Computing 19 (2003) 479–500.
[18] J. Grooss, J. Hesthaven, A level set discontinuous Galerkin method for free surface flows, Computer Methods in Applied Mechanics and Engineering 195 (2006) 3406–3429, URL http://www2.imm.dtu.dk/pubdb/p.php?3590.
[19] M.J. Berger, P. Colella, Local adaptive mesh refinement for shock hydrodynamics, Journal of Computational Physics 82 (1989) 64–84.
[20] A. Anderson, X. Zheng, V. Cristini, Adaptive unstructured volume remeshing I: THE method, Journal of Computational Physics 208 (2) (2005) 616–625.
[21] X. Zheng, J. Lowengrub, A. Anderson, V. Cristini, Adaptive unstructured volume remeshing II: application to two- and three-dimensional level-set simulations of multiphase flow, Journal of Computational Physics 208 (2) (2005) 626–650.
[22] M. Iskandarani, J. Levin, B.-J. Choi, D. Haidvogel, Comparison of advection schemes for high-order hp finite element and finite volume methods, Ocean Modeling 10 (1–2) (2005) 233–252.
[23] T.D. Aslam, A level set algorithm for tracking discontinuities in hyperbolic conservation laws II: systems of equations, Journal of Scientific Computing 19 (1–3) (2003) 37–62.
[24] J. Weideman, L. Trefethen, The kink phenomenon in Fejer and Clenshaw–Curtis quadrature, Numerische Mathematik (submitted for publication).

[25] L. Trefethen, Is Gauss quadrature better than Clenshaw–Curtis? SIAM Review (in press).
[26] B. Cockburn, C.-W. Shu, TVB Runge–Kutta local projection discontinuous Galerkin finite element method for conservation laws ii: General framework, Mathematics of Computation 52 (1989) 411–435.
[27] A. Patera, A spectral element method for fluid dynamics: laminar flow in channel expansion, Journal of Computational Physics 54 (3) (1984) 468–488.
[29] S. Gottlieb, C.W. Shu, E. Tadmor, Strong stability-preserving high-order time discretization methods, Siam Review 43 (1) (2001) 89–112.
[30] N. Chevaugeon, J. Xin, P. Hu, X. Li, D. Cler, J. Flaherty, M. Shephard, Discontinuous Galerkin methods applied to shock and blast problems, Journal of Scientific Computing 22 and 23 (2005) 227–243.
[31] L. Krivodonova, J. Xin, J.F. Remacle, N. Chevaugeon, J.E. Flaherty, Shock detection and limiting with discontinuous Galerkin methods for hyperbolic conservation laws, Applied Numerical Mathematics 48 (3–4) (2004) 323–338.
[32] D. Nguyen, F. Gibou, R. Fedkiw, A fully conservative ghost fluid method and stiff detonation waves, in: Proceedings of the 12th International Detonation Symposium, San Diego, CA, 2002..
[33] R. Baltensperger, M.R. Trummer, Spectral differencing with a twist, SIAM Journal on Scientific Computing 24 (5) (2003) 1465–1487.
[34] C.-W. Shu, S. Osher, Efficient implementation of essentially non-oscillatory shock-capturing schemes II, Journal of Computational Physics 83 (1) (1989) 32.
[35] J. Greenough, W. Rider, A quantitative comparison of numerical methods for the compressible Euler equations: fifth-order WENO and piecewise linear Godunov, Journal of Computational Physics 196 (1) (2004) 259–281.